Absorption and emission spectra of Ce^{3+} in elpasolite lattices

Peter A. Tanner* and Chris S. K. Mak
Department of Biology and Chemistry, City University of Hong Kong, Tat Chee Avenue, Kowloon, Hong Kong SAR. Peoples' Republic of China

Norman M. Edelstein* and Keith M. Murdoch
Chemical Sciences Division, Lawrence Berkeley National Laboratory, Berkeley, CA 94720-8175 USA

Guokiu Liu
Chemistry Division, Argonne National Laboratory, Argonne, IL 60439 USA

Jin Huang
Department of Physics and Astronomy, University of Wisconsin, Eau Claire, WI 54702, USA

Luis Seijo and Zoila Barandiarán
Departamento de Quíimica, C-XIV and Instituto Universitario de Ciencia de Materiales Nicolás Cabrera, Universidad Autónoma de Madrid, 28049 Madrid, Spain

E-mail: BHTAN@cityu.edu.hk; nmedelstein@lbl.gov

Abstract

The experimental determination of the electronic energy levels for Ce^{3+} in some chloro-elpasolite hosts for both the ground $4f^1$ and the excited $5d^1$ configurations are described. High resolution f - f absorption and f - $^2T_{2g}$ d absorption and emission spectra have been recorded at low temperatures for Ce^{3+} diluted into various hexachloroelpasolite lattices. A fluorescence spectrum at ~ 50,000 $cm^{-1}$is tentatively assigned to the emission from the highest 5d crystal field level , ^2E_g, of a Ce^{3+} impurity in $Cs_2NaErCl_6$, enabling the values of all the energy levels of both the $4f^1$ and $5d^1$ configurations to be given for

Ce^{3+} in elpasolite hosts. Vibronic structure superimposed on the electronic transitions is analyzed in terms of a simple configurational coordinate model involving the ground and excited configurations. It is found that the difference in the Ce-Cl bondlength between the $4f^1$ and $5d^1$ configurations is ~0.04Å. Ab initio model potential calculations on the $(CeCl_6)^{3-}$ cluster embedded in a reliable representation of the Cs_2NaYCl_6 host support these conclusions.

Introduction

At the beginning of the 4f and the 5f transition series, the f and d electronic configurations of the di-, tri-, and tetravalent free ions are very close in energy. [1,2] This is also true for these ions in compounds. For example, the lowest energy configuration for the Ce^{2+} free ion is [Xe core]$4f^2$ with the beginning of the opposite parity 4f5d configuration at 3277 cm^{-1}. However in a CaF_2 host the ground configuration is [Xe core]4f5d.[3] The Ce^{3+} free ion has a $4f^1$ ground configuration with the lowest 5d state at 49737 cm^{-1}.[1] When this ion is placed in a crystal the lowest 4f to 5d electric dipole allowed transition has been reported to be in the range of 20,000 to 40,000 cm^{-1} depending on the particular compound or matrix investigated.[4] Similarly, for the actinide or 5f series, the lowest 5f – 6d transition for the Pa^{4+} ion diluted in Cs_2ZrCl_6 is at 20,000 cm^{-1}, but the free ion separation between ground 5f level and the first 6d level is ~ 50,000 cm^{-1}. [5] In the few structurally characterized Th^{3+} organometallic compounds the $6d^1$ configuration has been found to be the ground configuration,[6,7] but the ground term is from the 5f configuration and the first 6d level is 10,000 cm^{-1} higher in the Th^{3+} free ion. The U^{3+} ion in the $LaCl_3$ host has the first $5f^3$ to $5f^26d^1$ transition at approximately 22,000 cm^{-1} although in the U^{3+}/RbY_2Cl_7 system this transition is found at ~ 14,000 cm^{-1}. [8] Thus, as the degree of ionization increases and/or the atomic number is increased (for both the lanthanide and the actinide series) the f^n configuration becomes increasingly stabilized so that the interconfigurational transitions are not observed in the visible or near ultraviolet region. Only at the beginning of both the lanthanide and actinide series is it possible to observe these two electronic configurations in this energy range.

For the lanthanide series the Ce^{3+} ion has been extensively studied and measured levels have been reported for both the ground $4f^1$ configuration and the excited $5d^1$ configuration. Figure 1 shows schematically the energy levels and nomenclature used for the $4f^1$ and $5d^1$ configurations of the Ce^{3+} ion diluted in choro-elpasolite hosts. The 6 K 4f-5d absorption and magnetic circular dichroism (MCD) spectra of Ce^{3+} diluted in Cs_2NaYCl_6 were reported by Schwartz and Schatz. [9] They located the 5d $^2T_{2g}$ Γ_8 and Γ_7 levels at 28196 $cm^{-1}$and 29435 cm^{-1} respectively. No further electronic absorption transitions were detected up to 50000 cm^{-1}. The 5d ^2E_g Γ_8 level was thus assumed to be >20000 cm^{-1} above the $^2T_{2g}$ baricenter. The EPR spectrum of the Ce^{3+} ion in Cs_2NaYCl_6 has also been measured.[10] The 5d-4f luminescence from the $^2T_{2g}$ state was recently reported under low resolution at 80 K, with about a 30 μs lifetime .[11] The decay curves for X-ray- and vacuum ultraviolet- excited emission of Ce^{3+}/Cs_2LiYCl_6 and $Ce^{3+}/Cs_2LiLaCl_6$ have recently been reported.[12,13] Ionova *et al.* have cited the lowest $\pi \rightarrow$ f charge transfer band in $CeCl_6^{3-}$ near 60000 cm^{-1}.[14]

van't Spijker et al,[15] reported the excitation spectra of the 425 nm (23530 cm^{-1}) emission of Ce^{3+} in $Cs_2NaLaCl_6$, $Cs_2NaCeCl_6$ and $Cs_2NaLuCl_6$. In each case, bands were observed near 210 nm and attributed to f – ^2E_g d transitions of Ce^{3+}. The wavelengths of these bands have been listed by Dorenbos,[16] with the addition of 210, 217 nm (47620, 46083 cm^{-1}) for Ce^{3+}/Cs_2NaYCl_6. The doublet structure (separation of the peak maxima ~ 1540 cm^{-1}) corresponded to absorption from both the $^2F_{5/2}$ and $^2F_{7/2}$ f-electron states to the d-electron ^2E_g state at room temperature. Hence it is well-substantiated that the ^2E_g state is near 47000 cm^{-1} in these cubic elpasolite hosts. This state also has been observed at 42200 cm^{-1} in the 300 K photoacoustic spectrum of Ce^{3+}/BaF_2.[17]

Rodnyi *et al.* [13] observed bands in the 300 K excitation spectrum of the 3.3 eV luminescence of Ce^{3+} in $Cs_2LiLaCl_6$ at 35730, 37908, 41134 and 45247 cm^{-1}, which were assigned to f – d transitions of Ce^{3+}. The 19 eV-excited emission spectrum of $Cs_2LiLaCl_6$ doped with 1% Ce^{3+} gave a broad band at 26616 cm^{-1}, assigned to d – f emission of Ce^{3+}, in addition to a broader feature (33069 cm^{-1}) assigned to core-valence luminescence. No emission was evident from the ^2E_g state of Ce^{3+}.

In a more recent study of Ce^{3+} - doped Cs_2LiYX_6, [18] even the neat Cs_2LiYCl_6 showed extensive bands between 48000-100000 cm^{-1} in the excitation spectra of the 'host'

emission at 29036 cm^{-1}. The 130 K excitation spectrum of Ce^{3+}/Cs_2LiYCl_6 (monitoring the Ce^{3+} emission at 25003 cm^{-1}) showed additional bands at roughly 27000-32000, 36300, 42700 and 50000 cm^{-1}. The 36300 and 42750 cm^{-1} bands were assigned to Ce^{3+} transitions: the lower energy band being due to a lower symmetry site, and the 50000 cm^{-1} band to the ^2E_g state. No emission was observed from the ^2E_g level in Ce^{3+} -doped Cs_2LiYX_6 under x-ray excitation, but emission from the $^2T_{2g}$ level was observed.

In this paper we report the experimental determination of the electronic energy levels for Ce^{3+} in some chloro-elpasolite hosts for both the ground $4f^1$ and the excited $5d^1$ configurations. A preliminary account of the emission spectra from the lowest 5d level of Ce^{3+} in Cs_2NaYCl_6 to the $4f^1$ energy levels has been given.[19] We have recorded an emission spectrum of $Cs_2NaErCl_6$ at ~ 50,000 cm^{-1}, which we tentatively assign to the emission from the highest 5d crystal field level of a Ce^{3+} impurity. Although the magnitude of the crystal field at the Ce^{3+} site in $Cs_2NaErCl_6$ is not quite the same as for Cs_2NaYCl_6 the differences should be relatively small since the ionic radii of Er^{3+} and Y^{3+} are similar. If the assumption is made that the differences in the crystal field strength are negligible, accurate data are available for both the $4f^1$ and $5d^1$ configurations in the elpasolite host. These data are analyzed and the parameters evaluated using the crystal field model.

We also report the results of supportive *ab initio* embedded cluster calculations[20,21] on $(CeCl_6)^{3-}/Cs_2NaYCl_6$.

Experimental

$Cs_2NaCeCl_6$ and other (Ce-doped) hexachloroelpasolites were prepared according to Morss method E.[22] The powders were passed through a Bridgman furnace at *ca*. 850 ^oC in vacuo in quartz tubes to give polycrystalline materials. The purity of the lanthanide oxides employed was 99.999% for Pr_6O_{11}, 99.9% Tm_2O_3, 99.999% Er_2O_3 (all from Strem Chemicals), and 99.999% Y_2O_3 (Berkshire Ores). $CeCl_3$ (99.9%, Strem) was used to prepare neat $Cs_2NaCeCl_6$ and Ce-doped Cs_2LiYCl_6. ICP-AES analyses showed that the Y_2O_3 contained (relative to Y) 58 ppm Ce, 120 ppm Pr, and 17 ppm Nd. Similar

analyses, by direct calibration and by standard addition, were attempted for the Er_2O_3 material but reliable data could not be obtained.

Infrared and absorption spectra were recorded using a Biorad FTS-60A spectrometer, equipped with DTGS and photomultiplier detectors, and using an Oxford Instruments closed-cycle cryostat with base temperature 10 K. Ultraviolet and emission spectra were also recorded using a D_2 lamp, or 355 nm radiation from a Nd-YAG laser, together with a 0.5 m Acton monochromator equipped with a charge-coupled device. Raman spectra were recorded as described previously.[23] Some experiments were also performed at Hong Kong University, where the Stokes H_2-shifted harmonics of a Nd-YAG pulsed laser were used to excite polycrystalline Ce/Cs_2NaYCl_6 and $Cs_2NaErCl_6$ (assumed to contain traces of Ce^{3+}) with the equipment described earlier.[24] The spectral resolution was between 2-4 cm^{-1}. Spectral calibration was performed using various standard lamps and the wavelengths were corrected to vacuum.

Fluorescence spectra obtained at LBNL from the lowest 5d level to the 4f manifolds were obtained using a Xenon lamp as described previously.[25] The sample was cooled to ~ 10 K using an Oxford Instruments model 1204 cryostat. The entrance and exit slits of the Spex 1403 double monochromator were set at 200 μm for a resolution on the order of 1 cm^{-1}. The spectra were calibrated with a mercury lamp and corrected to vacuum.

Review of parametric theory

The Hamiltonian for the energy levels of an *f* electron in an octahedral crystal field may be written as [26]

$$H = H_{SO} + H_{CF}$$

$$H_{SO} = \zeta_{4f}(r)\, \mathbf{l}\cdot\mathbf{s}$$

$$H_{CF} = B_0^4\left[C_0^4 + (5/14)^{1/2}(C_{-4}^4 + C_4^4)\right] + B_0^6\left[C_0^6 - (7/2)^{1/2}(C_{-4}^6 + C_4^6)\right]. \qquad (1)$$

The empirical parameters above include the crystal field parameters B_0^4 and B_0^6, (utilizing the Wybourne notation) and the spin-orbit coupling constant $\zeta_{4f}(r)$. The matrix elements for the angular momentum operators **s** and **l** and the tensor operators C_q^k depend only on the angular coordinates and are evaluated by standard techniques.[26,27] For the $4f^1$ configuration of Ce^{3+}/Cs_2NaYCl_6, the spin-orbit interaction is larger than the crystal field interaction. The spin-orbit coupling interaction splits the f^1 free ion state into two J levels, J=5/2 and 7/2, and the octahedral crystal field splits the ground J = 5/2 term into a Γ_{7u} doublet and a Γ_{8u} quartet, using the double group notation for octahedral symmetry. Similarly the J = 7/2 term splits into two doublets of Γ_{7u} and Γ_{6u} symmetry and one quartet of Γ_{8u} symmetry. Figure 1 shows the approximate energy level diagram and the nomenclature used.

The above Hamiltonian may also be utilized for the 5d configuration. In this case the sixth order crystal field term B_0^6 is equal to zero and the spin-orbit coupling constant is $\zeta_{5d}(r)$. However, unlike for the 4f configuration, the 5d configuration experiences a crystal field interaction that is considerably larger than the 5d spin-orbit coupling. The octahedral (O_h) crystal field splits the $5d^1$ configuration into two levels, a triply orbitallydegenerate T_{2g} lower state and a doubly orbitally degenerate E_g upper state. When the spin-orbit interaction is included, the T_{2g} level splits into a quartet Γ_{8g} lower level and a higher-lying doubly degenerate Γ_{7g} state. The E_g upper state transforms into a quartet Γ_{8g} state as shown in Figure 1. The solutions of the above Hamiltonian for a $4f^1$ or a $5d^1$ electron configuration are well known and will not be repeated.[28]

The emission and absorption transitions reported in this paper between the $4f^1$ and $5d^1$ configurations are allowed electric dipole transitions that originate or terminate either in crystal field states of Γ_{7u}, Γ_{8u}, or Γ_{6u} symmetry for the $4f^1$ configuration or Γ_{8g} or Γ_{7g} for the $5d^1$ configuration. The electric dipole operator transforms as Γ_{4u}. Evaluating the direct products of the initial and final states with the electric dipole operator shows all purely electronic zero phonon transitions are allowed, with the exception of Γ_{7g} - Γ_{6u}. The $f \leftrightarrow d$ transitions between Γ_7 states may couple with totally-symmetric vibrational modes, whereas in addition the τ_{2g} mode is potentially Jahn-Teller active between Γ_7 and Γ_8 states.

f-f absorption spectra

The $4f^1$crystal field levels of $Cs_2NaCeCl_6$ have been deduced from electronic Raman studies and are given in Table 1.[23,29] A crystal field fit gave $\zeta_{4f} = 623$ cm^{-1}, $B_0^4 = 2119$ cm^{-1} and $B_0^6 = 261$ cm^{-1}.[30] The f-f electronic absorption spectrum of Ce^{3+}/Cs_2NaYCl_6 and $Cs_2NaCeCl_6$ have been reported and are dominated by magnetic dipole transitions.[31] Although the former is cubic at low temperatures, the latter undergoes a phase transition at 178 K.[10,32-34] The infrared absorption spectra were reinvestigated in this study and the derived energy levels are listed in Table 1. The magnetic dipole transitions $(^2F_{5/2})\Gamma_7 \rightarrow (^2F_{7/2})\Gamma_7$, Γ_8 are the most intense bands, with measured oscillator strengths 4.8×10^{-8} and 5.1×10^{-8} respectively in dilute Ce^{3+}/Cs_2NaYCl_6. The fact that values measured in neat $Cs_2NaCeCl_6$ are smaller (6.3×10^{-9} and 1.7×10^{-8}, respectively) is attributed to saturation effects.

Vibrational spectra

The normal vibrations of the $Cs_2NaCeCl_6$ crystal are described in the notation of Lentz, with the relationship to the $CeCl_6^{3-}$ moiety mode vibrations being given in Table 2.[35] Assignments are included from the Raman and vibronic spectra. The energies of the stretching vibrations are somewhat higher in the Cs_2NaYCl_6 lattice, with ν_1, for example, being near 300 cm^{-1}. Also included in Table 2 are the results from normal coordinate calculations employing moiety mode and unit cell group models.[36,37]

$4f^1\ ^2F_{5/2}$ - $5d^1$ ($^2T_{2g}$) absorption spectra

The 6 K ultraviolet electronic absorption spectrum of Ce^{3+}/Cs_2NaYCl_6 has previously been reported by Schwarz and Schatz.[9] It comprises electric-dipole allowed transitions from the $4f^1\ ^2F_{5/2}\ \Gamma_{7u}$ ground state to the $5d^1\ ^2T_{2g}\ \Gamma_{8g}$ and Γ_{7g} states. Prominent vibrational progressions in modes of 300 cm^{-1} and 47 cm^{-1} were built upon the zero

phonon lines. We have reinvestigated the spectra at 10 K, and our spectrum is very similar to that of Schwarz and Schatz, with fine structure in addition to the two prominent progressions. A further progression in a lattice mode of ca. 14-16 cm^{-1} was reported by Schwarz and Schatz, although the first member is not evident in the present study or in their published spectrum. However, we do observe a shoulder at 32 cm^{-1} above the zero phonon line, in agreement with Schwarz and Schatz.

The 10 K absorption spectra of *neat* $Cs_2LiPrCl_6$ and $Cs_2LiTmCl_6$ in the ultraviolet show f-d absorption bands due to Ce^{3+} impurities (Fig. 2). The zero phonon line transition energies are listed in Table 3. The weak feature to low energy of $\Gamma_{7u} \rightarrow \Gamma_{8g}$ in $Ce^{3+}/Cs_2LiPrCl_6$ is a hot band. The low energy part of $Ce^{3+}/Cs_2LiTmCl_6$ absorption spectrum overlaps the $^3H_6$-$^1D_2$ f-f transition of $Cs_2LiTmCl_6$. Samples of elpasolite hosts doped with Ce^{3+} concentrations of the order of 1% exhibit total absorption in this region. The vibrational progression frequencies, averaged over all the first members, are listed for the two strongest progression modes in Table 4.

$^2T_{2g}$ $5d^1$ -$4f^1$ $^2F_{5/2}$, $^2F_{7/2}$ emission spectra

The Xe lamp-excited ~10 K emission spectrum of dilute Ce^{3+}/Cs_2NaYCl_6 is shown in Figure 3. Transitions are observed to the $^2F_{5/2}$, $^2F_{7/2}$ terminal crystal field levels of Ce^{3+}, as marked in Figure 3, and the derived energies are listed in Table 5. The lowest energy electronic origin is mostly self-absorbed, as is shown by the superposition of the absorption and 199.8 nm excited emission spectra from the $5d^1$ level, both at 10 K (Figure 4). The mirror-image relationship of the absorption and emission spectra is not exact because, although the 0-0 transitions coincide, there are further electronic transitions which are unique to either absorption or emission. The energy difference between the maxima in the emission and absorption spectra, *ca*. 1920 cm^{-1}, is therefore not solely related to vibrational energies, but also to the locations of the relevant $5d^1$ and $4f^1$ electronic states.

The D_2-lamp and 355 nm excited luminescence spectra of Ce^{3+}/Cs_2NaYCl_6 at 10 K are similar to the 199.8 nm-excited spectrum, except that the highest energy bands are strongly self-absorbed. The 199.8 nm-excited emission spectrum of Ce^{3+} doped into

Cs_2LiYCl_6 is generally similar to, but less well-resolved than, the spectrum of Ce^{3+}/Cs_2NaYCl_6 (Figure 5).

An additional, very weak, group of bands (not shown here) is observed in the 355 nm excited spectrum of Ce^{3+}/Cs_2NaYCl_6, with the highest energy electronic origin at 22210 cm^{-1}. Based upon this zero phonon line, progressions in vibrational modes of 274 and 173 cm^{-1} are observed to low energy. Since the former energy is rather less than the Ce-Cl vibrational frequency of $CeCl_6^{3-}$, and these bands are located at *ca.* 3300 cm^{-1} below the 5d - 4f electronic transition energy, a probable assignment is to the one quantum of the O-H vibration based upon the (unobserved) 5d - 4f zero phonon line of this trace impurity, partially hydrolysed $CeCl_6^{3-}$ ion.

^2E_g $5d^1$-$4f^1$ emission spectra

Under 199.8 nm excitation at 10 K, a group of bands is observed in the emission spectrum of neat $Cs_2NaErCl_6$ which cannot be associated with electronic transitions of Er^{3+} (Figure 6). We tentatively assign this emission to the Ce^{3+} $5d^1$ ^2E_g state emitting to the $4f^1$ electronic levels. The reasons for this assignment are because (i) the luminescence is clearly d - f and not f - f, and there are no $f^{10}d$ energy levels of Er^{3+} at such low energy; (ii) f - f luminescence from Er^{3+} would be quenched by the $^4D_{1/2}$ state, just below 47000 cm^{-1}; (iii) the line intervals cannot be matched with energy level intervals of $ErCl_6^{3-}$. Furthermore, these bands are not evident in the emission spectrum of dilute Er^{3+}/Cs_2NaYCl_6, nor in the 218-nm excited spectra of $Cs_2NaErCl_6$. The electronic origin at highest energy is located at 47080 cm^{-1} (Figure 6). The progressions in vibrational modes of 49 cm^{-1} and 297 cm^{-1} are characteristic of the 5d - 4f emission spectra described above. At the second member of the ν_1 progression there is an apparent doubling of bands, which can be explained by the presence of a further electronic state at 594 cm^{-1} above the ground state. It is for these reasons that we believe these bands can be assigned to emission from the d^1 ^2E_g Γ_8 state of a Ce^{3+} impurity in neat $Cs_2NaErCl_6$.

Only one further similar group of bands is observed to lower energy. For this weaker group of bands (Fig. 6), two further electronic origins can be assigned. The inferred

locations of the $4f^1\ ^2F_{7/2}$ states (Table 5) are however, rather lower (by about 40 cm^{-1}) than expected from the energy levels of Ce^{3+}/Cs_2NaYCl_6.

Since the 199.8 nm excitation energy is 2954 cm^{-1} to high energy of the highest energy zero phonon line of Ce^{3+}, it appears that either the absorption takes place into an Er^{3+} energy level, with subsequent energy transfer to Ce^{3+}; or that cooperative ion effects occur. Strong emission from the 4f-energy levels of Er^{3+} is observed at lower energies, which masks the $^2T_{2g}$ Ce^{3+} transitions, if present.[24]

We have assigned the fluorescence spectra observed in $Cs_2NaErCl_6$ beginning at 47080 cm^{-1} as the emission from the highest $5d^1$ E_g level to the 4f levels of the Ce^{3+} ion. This assignment is consistent with other observations for the Ce^{3+} ion in this energy range as discussed in the introduction. The observed vibronic spectra and the derived 4f energy levels given in Table 1 support this assignment. However no fluorescence from the E_g state was observed in the Ce^{3+}/Cs_2NaYCl_6 system when this system was excited in the wavelength range of 192-210 nm at 10 K, although T_{2g} emission was observed. The calculated E_g emission intensities are in poor agreement with the experimental data (see below). One possibility for the quenching of the E_g emission in the Ce^{3+}/Cs_2NaYCl_6 system is by energy transfer to killer sites. The most likely candidates are Pr^{3+} and/or Nd^{3+} since these ions have 5d levels in the 200 nm region. Analysis of the undoped Cs_2NaYCl_6 crystal shows that these ions are present in relatively significant concentrations, so this is a possibility. Reliable analytical data could not be obtained for the Er_2O_3 starting material used to prepare $Cs_2NaErCl_6$. If the amount of Pr/Nd in the $Cs_2NaErCl_6$ crystal is significantly less than in the Cs_2NaYCl_6 system, then this could be a possible explanation for the appearance of the $5d^1$ E_g emission. The fluorescence from the Ce^{3+} E_g state is unlikely to be quenched by Er^{3+} f-electron levels. Quenching by d-electron levels of Nd^{3+}/Pr^{3+} would not give rise to d - f emission from these lanthanide ions because Nd^{3+} does not exhibit d - f emission in elpasolites, and Pr^{3+} d - f emission is quenched by Ce^{3+}.

Vibrational progressions, linewidths and Condon parabolae

Several vibrational progressions have been identified above in the $^2T_{2g}$ $5d^1$ - $4f^1$ $^2F_{5/2}$, $^2F_{7/2}$ emission and absorption spectra of $CeCl_6^{3-}$. Selection rules for these spectra show that the vibrational mode must transform as the totally symmetric representation at the O_h crystal site of Ce^{3+}. Following the remarks of Schwartz and Schatz,[9] and by comparison of the progression intervals with Table 2, it is clear an alternative, the occurrence of Jahn-Teller effects, is not evident in the $^2T_{2g}$ state. These authors assigned vibrational progression modes with energies of 16 and/or 32 cm^{-1}. The first of these energies is comparable with the S_3 rotatory mode, whereas the second energy could correspond to an acoustic mode. The occurrence of progressions in these modes would thus infer contributions to the intensity from points away from the zone center. Since these progressions are not well-resolved, and we do not observe corresponding features in the spectra of $Ce^{3+}/Cs_2LiLnCl_6$, we do not discuss these bands further. The strongest progressions in the spectra of Ce^{3+}/Cs_2ALnCl_6 (A = Na, Li) occur in the ν_1 (α_{1g}) $CeCl_6^{3-}$ moiety (*i.e.* first shell) mode, with the energy rather greater than in neat Cs_2ACeCl_6 because $CeCl_6^{3-}$ is compressed in the crystalline hosts employed. The next prominent progression occurs in the mode near 44-49 cm^{-1} in A = Na hosts, but in 51-54 cm^{-1} in A = Li hosts. Clearly the energy of this mode is not very sensitive to the masses of Ln or A, but it is similar to that of the S_5 (τ_{2g}) mode. This progression mode can therefore be envisaged as a $\mathbf{k} \neq 0$ totally symmetric mode (such as along the Δ direction of reciprocal space), or more simply (but less accurately) as the totally symmetric stretch of the second shell, $CeCs_8$.

It is evident that a further, weaker progression occurs in a vibrational mode of 180-193 cm^{-1} for A = Na, and 237-252 cm^{-1} for A = Li. This vibration can be envisaged as the contribution from the S_8 (τ_{1u}) mode away from the zone center, or alternatively, from the totally symmetric stretch of the third shell, $Ce\text{-}Na_6$. In all of these totally symmetric breathing modes, the Ce nucleus is stationary. Additional evidence for this latter "sodium" mode comes from the study of the linewidths and relative intensities of consecutive bands in the emission spectra. Considering the emission transition $^2T_{2g}$ Γ_{8g} $\rightarrow$ $^2F_{5/2}$ Γ_{8u}, after subtraction of the continuous background, the first few bands can be better fitted by Gaussian rather than Lorentzian profiles (Fig. 7). This is presumably because some of the fitted bands comprise more than one component. The half-height

width shows an increase for the first few bands in the progression of the 48 cm^{-1} lattice mode, with a progressive decrease in intensity. A sharper feature is then apparent at 190±3 cm^{-1}, which must then correspond to the first member of a further progression. The lowest energy band in Figure 7 corresponds to the first member of the 48 cm^{-1} lattice mode progression upon the 190 cm^{-1} mode.

The wavefunctions obtained from Eq. (1) represent only the pure electronic wavefunctions. Considering also vibronic coupling, the intensity of an electronic transition from the initial state *i* to the final state *f* may be written (in the adiabatic approximation which assumes the electronic part is independent of the vibrational coordinates) as

$$I \propto |\langle i|e\mathbf{r}|f\rangle\langle l|m\rangle|^2 \qquad (2)$$

where *I* is the intensity, $e\mathbf{r}$, the electric dipole operator, and *l* and *m* are the initial and final vibrational states, respectively.[38,39] If it is further assumed that the electronic-vibrational coupling is linear (i.e., the vibrational states in the ground and excited states are equal), and only the lowest vibrational level of the initial state is populated, then

$$I_n \approx e^{-S_{H-R}}\left(\frac{S_{H-R}^n}{n!}\right), \qquad (3)$$

where $S_{H\text{-}R}$ is the Huang-Rhys parameter and *n* is the vibrational quantum number of the terminal state.

The Huang-Rhys parameter can be evaluated from a harmonic progression in a vibrational mode. For the vibration corresponding to the normal coordinate Q_i,

$$S_{H\text{-}R} = \frac{M\omega_i}{2\hbar}(\Delta Q_i)^2 \qquad (4)$$

where M is the effective mass and ΔQ_i is the difference between the equilibrium distances of the metal ion and the ligand in the ground and excited states for the vibrational mode ν_i of angular frequency ω_i.[38,39]

A similar method to relate the change in intensity along a vibrational progression to the change along the corresponding vibrational coordinate has been given by Yersin *et al.*[40] They have related the measured, relative vibronic intensities in emission $I^{0,n}$ and absorption $I^{m,0}$ (where m,n indicate the number of quanta) to the zero phonon line (ZPL) intensity, $I^{0,0}$. For the case of the ν_1 progressions:

$$\frac{I^{0,n}}{I^{0,0}} = \left[\frac{E(ZPL) - n\nu_1}{E(ZPL)}\right]^4 \left[\frac{R_{0,n}}{R_{0,0}}\right]^2 \quad \text{.....} \quad \text{(5a)}$$

$$\frac{I^{m,0}}{I^{0,0}} = \left[\frac{E(ZPL) + m\nu_1}{E(ZPL)}\right] \left[\frac{R_{m,0}}{R_{0,0}}\right]^2 \quad \text{.....} \quad \text{(5b)}$$

where the overlap integrals $R_{0,n}$ and $R_{m,0}$ can be related to the displacement ΔQ of the minimum of the potential surface of the excited electronic state along the α_{1g} normal coordinate. Furthermore, the individual Ce-Cl bond length change, $\Delta r = \Delta Q/\sqrt{6}$. The Franck-Condon analyses were performed upon the emission and absorption spectra, after subtraction of the continuous background.[41]

The spectra shown in Figure 8 were fit by using the Huang-Rhys formulation for three oscillators, $S_{H\text{-}R1}$ corresponding to the ~ 300 cm^{-1} ν_1 vibration, $S_{H\text{-}R2}$ corresponding to the ~48 cm^{-1} assigned to the totally symmetric stretch $\nu_{lattice}$ vibration. The third frequency $S_{H\text{-}R3}$ was used to fit the broad background. The line widths were treated as free parameters and the relative intensities of the two electronic transitions involved, $^2T_{2g}$ (or E_g) $\Gamma_{8g} \rightarrow {}^2F_{5/2}$ Γ_{7u} and $^2T_{2g}$ (or E_g) $\Gamma_{8g} \rightarrow {}^2F_{5/2}$ Γ_{8u}, were adjusted to give the best fit. Representative fits for the ~28000 cm^{-1} emission of $Ce^{3+}/Cs_2NaYnCl_6$ (from Fig. 3a) and for the ~48000 cm^{-1} emission of $Ce^{3+}/Cs_2NaErCl_6$ (from Fig. 6) are shown in Figure 8. Franck-Condon analyses using Eqs. 5a and 5b also were performed upon all the emission and absorption spectra, after subtraction of the continuous background[41] assuming that the vibrational frequencies are unchanged in the ground and excited states.

The derived parameters, Δr and ΔQ are listed in Table 4. The displacement between the d- and f-electron potential energy hypersurfaces of 0.09-0.13 Å, represents a Ce-Cl bond length change of about 0.04 Å, which is <2% of the bond length. Similar changes have been obtained from the analysis of 5d → 4f emission transitions of Pr^{3+} in elpasolite lattices.[42] The bond length change along the Cs^{+} lattice mode coordinate from this analysis is 0.05-0.07 Å.

A similar fit was performed for the ~ 50,000 cm^{-1} emission assigned (tentatively) as due to the $^2E_g\ \Gamma_8 \rightarrow {}^2F_{5/2}$. With this initial state the displacement between the d- and f-electron potential energy hypersurfaces is 0.08-0.09Å, representing a Ce-Cl bond length change of about 0.035 Å, slightly smaller than found with the $^2T_{2g}\ \Gamma_8$ as the initial state. The differences in bond distances found for transitions that are initiated from either the T_{2g} or the E_g orbitals can be rationalized by the differences in bonding in these two 5d orbitals (see below).

Electric dipole intensities and crystal field calculations

The wavefunctions obtained from diagonalization of the matrices given by Eq. 1 can be used to evaluate Eq. 2. The radial part of Eq. 2 is the same for all transitions so we compare the calculated relative intensities with the measured relative intensities for the emission transitions in Table 6.

The measured electric dipole intensities from the $T_{2g}\ \Gamma_8$ state to the 4f levels were obtained by subtracting an empirical background corresponding to the underlying broad background shown in Figure 3 from the spectra and then fitting the vibronic peaks with a Gaussian peak-fitting program. We estimate the accuracy of the experimental intensities obtained in this way to be about 50%. For transitions originating from the lowest level of the $5d^1$ configuration, the agreement between the experimental and calculated relative intensities is reasonable.

With the assumption that Figure 6 corresponds to emission from the ^{2}Eg state of Ce^{3+}, then the relative intensities of transitions from this level are not in good agreement with calculation. This is not because the lower energy bands are absorbed by Er^{3+} transitions

in $Cs_2NaErCl_6$, since there is a spectral window between 44000-46000 cm^{-1} for the energy levels of Er^{3+}.

The calculated intensities show that the emission to the $4f^1\ ^2F_{7/2}$ states should be considerably greater from the $5d^1\ E_g$ levels than from the $5d^1\ T_{2g}$ levels. The reason for this intensity change is because only transitions with $\Delta J = 0,\pm1$ are allowed. The $5d^1\ E_g$ wavefunctions have ~65% L =3, J = 5/2 character and ~35% L =3, J = 3/2 character as compared to the ~35% L =3, J = 5/2 character and ~65% L =3, J = 3/2 character of the $5d^1\ T_{2g}$ wavefunctions. Thus for the $5d^1\ T_{2g}$ wavefunctions, the major component of the wavefunctions can not contribute any intensity (in the limit of zero crystal field mixing) to the $4f^1$ J = 7/2 levels. Nevertheless, the experimental intensities from the $5d^1\ E_g$ levels are completely off from the calculated values. In fact the calculated values show the intensities to the $4f^1$ J=7/2 states should be larger than to the $4f^1$ J=5/2 states, completely in reverse to the observed values.

As expected the crystal field fits shown in Table 5 agree with the experimental energies quite well. In this case the number of observables and the number of parameters are comparable. A better test is the comparison of the calculated ground state $4f^1\Gamma_{7u}$ g value g = -1.253 with the experimental value, g = |1.266|.[10]

Ab initio calculations

In order to complement the data with independent theoretical information, we performed wave function based *ab initio* calculations on the $(CeCl_6)^{3-}$ cluster embedded in a reliable representation of the Cs_2NaYCl_6 host. The results are summarized in Table 7. These calculations take into account the most important bonding interactions within the $(CeCl_6)^{3-}$ unit, including electron correlation and scalar and spin-orbit coupling relativistic effects, and Cs_2NaYCl_6 host embedding effects.

The details of the calculations follow. We use the *ab initio* model potential method, AIMP, as an embedding technique and as an effective core potential method.[20,21] The embedding potential we use for Cs_2NaYCl_6 was obtained earlier.[43] The relativistic AIMP we use for Ce was obtained from Seijo[44] and represents its [Kr] core; the *ab initio* spin-orbit potential produced earlier [45] is used here with an empirical scaling factor 0.9;[46] the

basis set for the 4d5s5p4f5d valence is the (14s10p10d8f)/[6s5p6d4f] set.[44] For Cl, we use the [Ne] core AIMP and the (7s6p) basis set[47] extended with one diffuse *p*-function[48] and contracted as [3s4p]. Additional (7s4p)/[1s1p] basis set functions are located on the Na^+ ions along the 100, 010, and 001 directions that are next neighbors to the $(CeCl_6)^{3-}$ cluster.[43] The electron correlation effects from the 36 3p electrons of the Cl ligands and the unpaired electron of Ce^{3+} are included by means of Average Coupled Pair Functional Calculations, ACPF.[49,50] Finally, we use the spin-free-state-shifted spin-orbit Hamiltonian (sfss)[51] in an identical manner as described [52] for $(PaCl_6)^{2-}$, in order to put together the electron correlation effects and the spin-orbit coupling effects in a simplified way.

The calculated bond distances along the breathing mode shown in Table 7 are almost equal for all the states of the $4f^1$ manifold; the slightly smaller values of the two Γ_{7u} sates correspond to them being the only ones with $4f(a_{2u})$ orbital character, which is the f orbital most stabilized by the ligand field. All these states have essentially the same ν_1 vibrational frequency. The computed values compare well with the experimental data. The computed minimum-to-minimum energy differences are very reasonable when compared with experiment; in order to lower the mean average deviation from 260 cm^{-1} it would probably be necessary to increase the methodological and computational demands to a very large extent. A more detailed analysis of these differences shows that its main contribution comes from a slight excess stabilization of the $4f(a_{2u})$ molecular orbital, (e.g. the mean average deviation from experiments is 80 cm^{-1} for the Γ_{8u} and Γ_{6u} states, with no $4f(a_{2u})$ contribution) which indicates that these calculations may be slightly overestimating the effective ligand field.

The calculations on the $5d^1$ manifold are perhaps more interesting. The bond distance of the two $^2T_{2g}$ states, Γ_{8g} and Γ_{7g}, are the same and smaller than the bond distance of the $4f^1$ states. The absolute value of the offset, 0.047 Å agrees well with the experimentally deduced value in Table 4. The fact that it is negative could not have been deduced from the analysis of the emission band shapes, which leads only to absolute values. The prediction of a cluster contraction in the transition from 4f to $5d(t_{2g})$ was also made in the corresponding case [52] of Pa^{4+}; it has to be the result of a balance between opposite tendencies: to increase bond distance as a consequence of the larger size of the 5(6)d

orbital, on the one hand, and to reduce bond distance as a consequence of the larger bond covalency in the $5(6)d^1$ states, on the other. An analysis of the detailed reasons leading to this contraction has been presented elsewhere.[53] The bond distance of the $5d^1\ ^2E_g\ \Gamma_{8g}$ is larger than that of the $^2T_{2g}$ states, as usual for the O_h ligand field splitting of d states and corresponding to the $5d(e_g)$ orbital being destabilized with respect to the $5d(t_{2g})$. The bond distance increases so as to make it larger than the $4f^1$ bond distances by 0.017 Å. The calculated vibrational frequencies are very similar to the $4f^1$ ones, only very slightly smaller, and they are again close to the approximate experimental value of 300 cm^{-1} deduced from absorption and MCD spectra of Ce^{3+}/Cs_2NaYCl_6. The minimum-to-minimum energies from the ground state to the two $^2T_{2g}$ states, Γ_{8g} and Γ_{7g}, are 2700 cm^{-1} too low, which is a reasonable result for a theoretically demanding 4f → 5d transition. Finally, the energy of the $5d^1\ ^2E_g\ \Gamma_{8g}$ state is calculated to be 47260 cm^{-1}. It agrees extremely well with the experimental observation in $Ce^{3+}/Cs_2NaErCl_6$, very probably as a consequence of compensation between an underestimation of the 4f → 5d baricenter and an overestimation of the ligand field, as already observed in the splitting of the $4f^1$ manifold. In any case, the *ab initio* calculation strongly suggests the existence of the $5d^1$ $^2E_g\ \Gamma_{8g}$ state of the $(CeCl_6)^{3-}$ unit 46000-48000 cm^{-1} above the ground state. This independent result supports the assignments of the emission spectrum of $Ce^{3+}/Cs_2NaErCl_6$ in Fig. 6.

Discussion and Conclusions

In this paper we have reported the results of detailed spectroscopic investigations of the Ce^{3+} ion in chloro-elpasolite hosts. The complete energy level schemes for the $4f^1$ and $5d^1$ configurations may be inferred from a combination of the fluorescence and absorption data from our work with earlier absorption data. Good fits were obtained for both the 4f and 5d levels using the crystal field model. However, although the calculated emission intensities from the 5d T_{2g} Γ_8 level were in reasonable agreement with the experimental intensities, the calculated intensities from the 5d E_g Γ_8 level were completely off. It is possible that admixtures of charge transfer states into the 5d E_g state could be important.

Theoretical calculations are presented which give reasonable agreement with the experimental energy levels and support the assignment of the 47080 cm^{-1} feature to the $5d^1$ E_g level. These calculations also show that the change in bond length between the $4f^1$ and $5d^1$ T_{2g} configuration is contractive with a value of ~0.04 Å, in excellent agreement with the experimental result (note that only the absolute value is obtained from the experimental results). This short bond for the 5d T_{2g} state suggests that the covalency of this 5d orbital with its consequent bond length shortening outweighs the lengthening of this bond due to the larger size of the 5d orbital. A detailed analysis for this has been presented elsewhere.[53] By contrast, the experimental measurements from the E_g emission spectrum show a slightly smaller bond length change than for the T_{2g} state. The theoretical calculations predict an increase in this bond length relative to that in the ground 4f configuration, which means a smaller bond length change than that obtained from the experimental analysis.

One factor that can account for some of these discrepancies hinges upon the subtraction of the broad background when integrating peaks in the emission or absorption spectra. Rather different results are obtained if the entire vibronic sideband is integrated (for example, in the Fig. 4 absorption spectrum, the maximum is at n = 1 if individual bands are considered, but at n = 2 quanta of ν_1 if the background is not subtracted). Although fits also were made assuming the background could be reproduced as a Gaussian function or by reproducing the background with a band coming from the Huang-Rhys equation with an empirical width, this may not necessarily account for the entire background. For example, (i) there are overlapping electronic transitions in some cases, and (ii) progressions in multiple quanta of odd vibrational modes may occur, partly giving rise to the broad underlying background. Furthermore, the relative intensities of the transitions involved with 47080 cm^{-1} emission were in disagreement with the predicted relative intensities obtained for the allowed electric dipole calculations. Thus the relative measured intensities from which the bond length changes are obtained must be considered somewhat suspect.

Acknowledgments

This research was supported in part by the Director, Office of Energy Research, Office of Basic Energy Sciences, Chemical Sciences Division of the U. S. Department of Energy under Contract No. DE-AC03-76SF00098 with the University of California. PAT acknowledges financial support for this study from the Hong Kong University Grants Commission Research Grant City U 1098/01P. LS and ZB acknowledge financial support from Ministerio de Ciencia y Tecnología, Spain (Dirección General de Investigación, BQU2002-01316). We are indebted to Dr. Kwok Wai-Ming for recording the 199.8 nm emission spectrum and to Dr. D. L. Phillips for the use of his laser laboratory. We also wish to thank Dr. M. F. Reid for performing the 5d – 4f intensity calculations reported in this paper.

References

(1) Martin, W. C.; Zalubas, R.; Hagan, L. *Atomic Energy Levels-The Rare-Earth Elements*; U.S. Government Printing Office, 1978.

(2) Fred, M. S. In *The Chemistry of the Actinide Elements*; 2nd ed.; Katz, J. J., Seaborg, G. T., Morss, L. R., Eds.; Chapman and Hall Ltd: London, 1986; Vol. 2, pp 1196-1234.

(3) Alig, R. C.; Kiss, Z. J.; Brown, J. P.; McClure, D. S. *Phys. Rev.* **1969**, *186*, 276.

(4) Dorenbos, P. *J. Lumin.* **2000**, *91*, 91.

(5) Edelstein, N. *Eur. J. Solid State Inorg. Chem.* **1991**, *28*, 47.

(6) Kot, W.; Shalimoff, G.; Edelstein, N.; Edelman, M. A.; Lappert, M. F. *J. Am. Chem. Soc.* **1988**, *110*, 986.

(7) Parry, J. S.; Cloke, F. G. N.; Coles, S. J.; Hursthouse, M. B. *J. Amer. Chem. Soc.* **1999**, *121*, 6867.

(8) Karbowiak, M.; Drozdzynski, J.; Murdoch, K. M.; Edelstein, N. M.; Hubert, S. *J. Chem. Phys.* **1997**, *106*, 3067.

(9) Schwartz, R. W.; Schatz, P. N. *Phys. Rev. B* **1973**, *8*, 3229.

(10) Schwartz, R. W.; Hill, N. J. *J. Chem. Soc. Faraday II* **1974**, 124.

(11) Laroche, M.; Bettinelli, M.; Girard, S.; Moncorgé, R. *Chem. Phys. Lett.* **1999**, *311*, 167.

(12) Combes, C. M.; Dorenbos, P.; van Eijk, C. W. E.; Krämer, K. W.; Güdel, H. U. *J. Lumin.* **1999**, *82*, 299.

(13) Rodnyi, P. A.; Mikhailik, V. B.; Stryganyuk, G. B.; Voloshinovskii, A. S.; van Eijk, C. W. E.; Zimmerer, G. F. *J. Lumin.* **2000**, *86*, 161.

(14) Ionova, G.; Krupa, J. C.; Gérard, I.; Guillaumont, R. *New J. Chem.* **1995**, *19*, 677.

(15) van't Spijker, J. C.; Dorenbos, P.; van Eijk, C. W. E.; Wickleder, M. S.; Güdel, H. U.; Rodnyi, P. A. *J. Lumin.* **1997**, *72-74*, 786.

(16) Dorenbos, P. *Phys. Rev. B* **2000**, *62*, 15650.

(17) Zhang, Y. G.; Don, Y. *Physica B* **1996**, *217*, 149.

(18) van Loef, E. V. D.; Dorenbos, P.; van Eijk, C. W. E.; Krämer, K. W.; Güdel, H. U. *J. Phys. Cond. Matter* **2002**, *14*, 8481.

(19) Edelstein, N. M. *J. Alloys and Compounds* **1995**, *223*, 197.

(20) Barandiarán, Z.; Seijo, L. *J. Chem. Phys.* **1988**, *89*, 5739.

(21) Seijo, L.; Barandiarán, Z. In *Computational Chemistry: Reviews of Current Trends, Vol. 4*; Leszczynski, J., Ed.; World Scientific: Singapore, 1999, pp 55.

(22) Morss, L. R.; Siegal, M.; Stenger, L.; Edelstein, N. *Inorg. Chem.* **1970**, *9*, 1771.

(23) Tanner, P. A.; Xia, S.; Liu, Y.-L.; Ma, Y. *Phys. Rev. B* **1997**, *55*, 12182.

(24) Tanner, P. A.; Chua, M.; Kwok, W.-M.; Phillips, D. L. *Phys. Rev. B* **1999**, *60*, 13902.

(25) Sytsma, J.; Murdoch, K. M.; Edelstein, N. M.; Boatner, L. A.; Abraham, M. M. *Phys. Rev. B* **1995**, *52*, 12668.

(26) Wybourne, B. G. *Spectroscopic Properties of Rare Earths*; Interscience Publishers: New York, 1965.

(27) Judd, B. R. *Operator Techniques in Atomic Spectroscopy*; McGraw-Hill: New York, 1963.

(28) Piehler, D.; Kot, W. K.; Edelstein, N. *Journal of Chemical Physics* **1991**, *94*, 942-948.

(29) Amberger, H.-D.; Rosenbauer, G. G.; Fischer, R. D. *Molec. Phys.* **1976**, *32*, 1291.

(30) Tanner, P. A.; Kumar, V. V. R. K.; Jayasankar, C. K.; Reid, M. F. *J. Alloys and Compounds* **1994**, *215*, 349-370.

(31) Tanner, P.; Krishnan, J. *Applied Spectroscopy* **1993**, *47*, 1522.

(32) Schwartz, R. W.; Watkins, S. F.; O'Connor, C. J.; Carlin, R. L. *J. Chem. Soc. Faraday II* **1976**, *72*, 565.

(33) Krupski, M. *Phys. Stat. Sol. (a)* **1989**, *116*, 657.

(34) Knudsen, G. P.; Voss, F. W.; Nevald, R.; Amberger, H.-D. In *Rare earths in Modern Science and Technology*; McCarthy, G. J., Silber, H. B., Rhyne, J. J., Eds.; Plenum: New York, 1982; Vol. 3, p 335.

(35) Lentz, A. *J. Phys. Chem. Solids* **1974**, *35*, 827.

(36) Tanner, P. A.; Shen, M. Y. *Spectrochim. Acta* **1994**, *50A*, 997.

(37) Ning, L. X.; Tanner, P. A.; Xia, S. D. *Vibrational Spectroscopy* **2003**, *31*, 51.

(38) Denning, R. G. In *Vibronic Processes in Inorganic Chemistry*; Flint, C. D., Ed.; Kluwer: Dordrecht, 1989; Vol. 288, p 111.

(39) Henderson, B.; Imbusch, G. F. *Optical Spectroscopy of Inorganic Solids*; Oxford University Press: Oxford, 1989.

(40) Yersin, H.; Otto, H.; Zink, J. I.; Gliemann, G. *J. Am. Chem. Soc.* **1980**, *102*, 951.

(41) Bron, W. E.; Wagner, M. *Phys. Rev.* **1965**, *139*, 233.

(42) Tanner, P. A.; Mak, C. S. K.; Faucher, M. D.; Kwok, W.-M.; Phillips, D. L.; Mikhailik, V. *Phys. Rev. B* **2003**, *67*, 115102.

(43) Al-Abdalla, A.; Barandiarán, Z.; Seijo, L.; Lindh, R. *J. Chem. Phys.* **1998**, *108*, 2005.

(44) Seijo, L.; Barandiarán, Z.; Ordejón, B. *Mol. Phys.* **2003**, *101*, 73.

(45) Seijo, L.; Barandiarán, Z.; Harguindey, E. *J. Chem. Phys.* **2001**, *114*, 118.

(46) Seijo, L. *J. Chem. Phys.* **1995**, *102*, 8078.

(47) Barandiarán, Z.; Seijo, L. *Can. J. Chem.* **1992**, *70*, 409.

(48) Dunning, J., T. H.; Hay, P. J. In *Modern Theoretical Chemistry*; Schaeffer III, H. F., Ed.; Plenum: New York, 1977, p 1.

(49) Ahlrichs, R.; Scharf, P.; Ehrhards, C. *J. Chem. Phys.* **1985**, *82*, 890.

(50) Gdanitz, R. J.; Ahrlrichs, R. *Chem. Phys. Lett.* **1988**, *143*, 413.

(51) Llusar, R.; Casarrubios, M.; Barandiarán, Z.; Seijo, L. *J. Chem. Phys.* **1996**, *105*, 5321.

(52) Seijo, L.; Barandiarán, Z. *J. Chem. Phys.* **2001**, *115*, 5554.

(53) Barandiarán, Z.; Seijo, L. *J. Chem. Phys.* **2003**, in press.

(54) Meyer, G. *Progr. Solid St. Chem.* **1982**, *14*, 141.

Figure captions

Fig. 1. Schematic energy level diagram of the $4f^1$ and $5d^1$ configurations of the Ce^{3+} ion in a chloroelpasolite crystal field. Note the change in the energy scale between the $4f^1$ and the $5d^1$ configurations.

Fig. 2. 10 K absorption spectra of trace Ce^{3+} impurity in $Cs_2LiPrCl_6$ and $Cs_2LiTmCl_6$ between 28000 - 31000 cm^{-1}. (The initial state is Γ_{7u} in all cases, and the terminal d-electronic states are labeled).

Fig. 3. 10 K UV xenon lamp excited emission spectrum of Ce^{3+}/Cs_2NaYCl_6 between 28500 - 22500 cm^{-1}

Fig. 4. Comparison of 10 K absorption spectrum of Ce^{3+}/Cs_2NaYCl_6 with the 199.8 nm excited emission spectrum at 10 K.

Fig. 5 Comparison of 199.8 nm excited 10 K emission spectra of (a) Ce^{3+}/Cs_2NaYCl_6 and (b) Ce^{3+}/Cs_2LiYCl_6. The terminal f-electron states are labeled.

Fig. 6. 199.8-nm excited 10 K emission spectrum of $Ce^{3+}/Cs_2NaErCl_6$ between 47000 - 43500 cm^{-1}.

Fig. 7. Gaussian fits to the first few bands in the 10 K $^2T_{2g}\ \Gamma_{8g} \rightarrow {}^2F_{5/2}\ \Gamma_{8u}$ emission spectrum of Ce^{3+}/Cs_2NaYCl_6. The numbers over the centers of the bands indicate the energy intervals (in cm^{-1}) from the zero phonon line.

Fig. 8. Fits of the experimental emission spectra using the Huang –Rhys formulation as described in the text. Top) Ce^{3+}/Cs_2NaYCl_6: $S_{H\text{-}R1}$=1.275, ω_1=299 cm^{-1}, line width=14 cm^{-1}; $S_{H\text{-}R2}$=1.8, ω_1=47.5 cm^{-1}, line width=14 cm^{-1}; $S_{H\text{-}R3}$= 4.39, ω_1=202 cm^{-1}, line width=145 cm^{-1}; intensity ratio of the transitions $^2T_{2g}\ \Gamma_{8g} \rightarrow {}^2F_{5/2}\ \Gamma_{7u}$ to $^2T_{2g}\Gamma_{8g} \rightarrow {}^2F_{5/2}\ \Gamma_{8u}$ = 2.0. Bottom) $Ce^{3+}/Cs_2NaErCl_6$: $S_{H\text{-}R1}$=1.13, ω_1=297 cm^{-1}, line width=9 cm^{-1}; $S_{H\text{-}R2}$=1.3, ω_1=48 cm^{-1}, line width=9 cm^{-1}; $S_{H\text{-}R3}$= 1.55, ω_3=300 cm^{-1}, line width=105 cm^{-1}; intensity ratio of the transitions $E_g\ \Gamma_{8g} \rightarrow {}^2F_{5/2}\ \Gamma_{7u}$ to $E_g\Gamma_{8g} \rightarrow {}^2F_{5/2}\ \Gamma_{8u}$ = 0.13. The calculated spectra are shown as the dotted lines, the experimental data are shown as solid lines. Gaussian line shapes are assumed.

Table 1. f-and d electron energy levels (in cm^{-1}) of Ce^{3+} in elpasolite lattices

Configuration $^{(2S+1)}L_J$	irrep	Electronic Raman, $Cs_2NaCeCl_6$ 20K	Electronic absorption, $Cs_2NaCeCl_6$ 90 K	Electronic absorption, Ce^{3+}/Cs_2NaYCl_6 10 K	Electronic absorption, $Ce^{3+}/Cs_2NaTmCl_6$ 90 K	Fluorescence $Ce^{3+}/Cs_2NaErCl_6$ 10 K	Fluorescence Ce^{3+}/Cs_2NaYCl_6 10 K	Fluorescence Ce^{3+}/Cs_2LiYCl_6 10 K
$4f^1\ ^2F_{5/2}$	Γ_{7u}	0	0	0	0	0	0	0
	Γ_{8u}	562, 580	563, 575	-	-	594	599	578
$4f^1\ ^2F_{7/2}$	Γ_{7u}	2161	2159	2159	2157	2125		
	Γ_{8u}	2663	2659	2674	(2676)	2628	2689	2674
	Γ_{6u}	3050	3048	-	-		3086	3061
$5d^1\ T_{2g}$	Γ_{8g}			28196			28193	28265
	Γ_{7g}			29435				
$5d^1\ E_g$	Γ_{8g}					47080		

Table 2. Vibrational assignments for $Cs_2NaCeCl_6$

Unit cell group mode and O_h point group irrep.	Moiety mode and O_h point group irrep.	20 K Raman spectrum	90 K f-f vibronic spectra	Calc.[b]	Calc.[c]
S_1 Ce-Cl sym. str.	ν_1 (α_{1g})	279	-	279	279
S_2 Ce-Cl str.	ν_2 (ε_g)	222	-	222	224
S_3 rotatory lattice (τ_{1g})	-	-	(~20)[a]	-	21
S_4 Cl-Ce-Cl bend	ν_5 (τ_{2g})	111	-	108	114
S_5 Cs transl. (τ_{2g})	-	46	-	-	48
S_6 Ce-Cl ant. str.	ν_3 (τ_{1u})	-	253(TO); 279(LO)	257	257
S_7 Cl-Ce-Cl bend	ν_4 (τ_{1u})	-	98(TO); 119(LO)	106	112
S_8 Na-Cl str. (τ_{1u})	-	-	(173)[a]	-	168
S_9 Cs transl. (τ_{1u})	-	-	56(TO); 69(LO)	-	53
S_{10} Cl-Ce-Cl bend	ν_6 (τ_{2u})	-	74-84	77	76

[a]From the spectra of $Cs_2NaPrCl_6$; TO/LO transverse/longitudinal optic modes; str. stretch; sym. symmetric; ant. antisymmetric; trans. translatory.[b] Using 5-parameter General Valence Force-Field for moiety modes.[36] [c]Using 9-parameter unit cell group model.[37]

Table 3. f-d absorption spectra of Ce^{3+} in elpasolite lattices

Lattice	Lattice parameter/Å[a]	Energy from $^2F_{5/2}\ \Gamma_{7u}$ (cm^{-1})		Energy difference (cm^{-1})
		$^2T_{2g}\ \Gamma_{8g}$	$^2T_{2g}\ \Gamma_{7g}$	
Cs_2NaYCl_6	10.733	28195±2	29435	1240
$Cs_2LiPrCl_6$	10.651	28363	29625	1262
$Cs_2LiTmCl_6$	10.439	28236	29489	1253
Cs_2LiYCl_6	10.479	28267	-	-

[a] From Meyer[54]

Table 4. Progression frequencies and bond length changes in f → d transitions of Ce^{3+} in elpasolite lattices

Crystal Host	Ce^{3+} concn. (mol %)	Transition	ν_1 (cm^{-1})	$\Delta Q(\nu_1)$ (Å) Ce-Cl	Δr (ν_1) (Å)[a]	ν(lat) (cm^{-1})	ΔQ(lat) (Å) Cs-Cl	Δr (lat) (Å)[a]
Emission								
Cs_2NaYCl_6	0.5	$^2T_{2g}\ \Gamma_{8g} \rightarrow {}^2F_{5/2}\ \Gamma_{8u}$	300±2	0.12	0.050	48±2	0.14	0.050
		$^2T_{2g}\ \Gamma_{8g} \rightarrow {}^2F_{5/2}\ \Gamma_{7u}$	298±3	0.11	0.046	48±2	0.14	0.050
b		$^2T_{2g}\ \Gamma_{8g} \rightarrow {}^2F_{5/2}\ \Gamma_{8u},\Gamma_{7u}$	299	0.09	0.037	47.5	0.139	0.049
Cs_2LiYCl_6	1.0	$^2T_{2g}\ \Gamma_{8g} \rightarrow {}^2F_{5/2}\ \Gamma_{8u}$	303±2	0.11	0.043	54±3	0.18	0.062
		$^2T_{2g}\ \Gamma_{8g} \rightarrow {}^2F_{5/2}\ \Gamma_{7u}$	301±1	0.12	0.049	52±3	0.15	0.053
$Cs_2NaErCl_6$	-	$E_g \rightarrow {}^2F_{5/2}\ \Gamma_{7u}$	297±5	0.10	0.040	49±3	0.15	0.055
b		$E_g \rightarrow {}^2F_{5/2}\ \Gamma_{8u},\Gamma_{7u}$	297	0.085	0.035	48	0.133	0.047
Absorption								
Cs_2NaYCl_6	0.01	$^2F_{5/2}\ \Gamma_{7u} \rightarrow {}^2T_{2g}\ \Gamma_{8g}$	299±2	0.13	0.051	44±3	0.15	0.054
$Cs_2LiTmCl_6$	-	$^2F_{5/2}\ \Gamma_{7u} \rightarrow {}^2T_{2g}\ \Gamma_{8g}$	296±5	-	-	54±3	-	-
$Cs_2LiPrCl_6$	-	$^2F_{5/2}\ \Gamma_{7u} \rightarrow {}^2T_{2g}\ \Gamma_{8g}$	285±5	0.13	0.051	51±2	0.19	0.067

[a] Absolute values of bond length difference between the 4f and 5d states involved in the particular transition
[b] Results from the Huang-Rhys analysis (see text)

Table 5. Derived f- and d- electron energy levels from the 10K emission spectra of $CeCl_6^{3-}$

State $nl^{1\ (2S+1)}L_J$	irrep.	Ce^{3+}/Cs_2NaYCl_6 (cm^{-1})	Ce^{3+}/Cs_2LiYCl_6 (cm^{-1})	$Ce^{3+}/Cs_2NaErCl_6$ (cm^{-1})	Calculated Levels (cm^{-1})[a,b,c]
$4f^1\ ^2F_{5/2}$	Γ_{7u}	0	0	0	0
	Γ_{8u}	599±3	578	594	597
$4f^1\ ^2F_{7/2}$	Γ_{7u}	-	-	2125	2167.
	Γ_{8u}	2689±3	2674	2628	2691
	Γ_{6u}	3086±3	3061	-	3085
$5d^1\ T_{2g}$	Γ_{8g}	28193±2	28265±3	-	28196
	Γ_{7g}	29435	-	-	29435
$5d^1\ E_g$	Γ_{8g}	-	-	47080	47125

[a]Data from Ce^{3+}/Cs_2NaYCl_6. For the $5d^1$ configuration the Γ_{7g} level was taken from Schwartz and Schatz[9] and the Γ_{8g} level from the $Ce^{3+}/Cs_2NaErCl_6$ data.

[b]Parameters (cm^{-1}) $4f^1$: $\zeta_{4f} = 624.1,\ B_0^4 = 2208.,\ B_0^6 = 249.6.$

$5d^1$: $F^0 = 36015.4,\ \zeta_{5d} = 792.7,\ B_0^4 = 38709.$

[c] $g(\Gamma_{7u})$ (calc) = 1.253.

Table 6 Relative experimental and calculated electric dipole emission intensities for $CeCl_6^{3-}$

	Relative Fluorescence Intensity from $5d^1\ T_{2g}\ \Gamma_{8g}$ [a] Experimental	Relative Fluorescence Intensity from $5d^1\ T_{2g}\ \Gamma_{8g}$ Calculated	Relative Fluorescence Intensity from $5d^1\ E_g\ \Gamma_{8g}$ [b] Experimental	Relative Fluorescence Intensity from $5d^1\ E_g\ \Gamma_{8g}$ Calculated
$4f^1\ ^2F_{5/2}\Gamma_{7u}$	.2	.76	1.0	1.0
$4f^1\ ^2F_{5/2}\Gamma_{8u}$	1.0	1.0	0.2	6.9
$4f^1\ ^2F_{7/2}\Gamma_{7u}$	-	.03	0.15	1.5
$4f^1\ ^2F_{7/2}\Gamma_{8'u}$	.05	.33	0.05	8.2
$4f^1\ ^2F_{7/2}\Gamma_{6u}$	.2	.30		5.3

[a] Ce^{3+}/Cs_2NaYCl_6

[b] $Ce^{3+}/Cs_2NaErCl_6$

Table 7 Ab initio embedded cluster calculations on Cs_2NaYCl_6:$(CeCl_6)^{3-}$.

Main character	State	r (ν_1) (Å)	Δr (ν_1) (Å)	ν_1 (cm^{-1})	T_e (cm^{-1})[a]	Experimental zero-phonon levels (cm^{-1})
$4f^1\ ^2F_{5/2}$	Γ_{7u}	2.723	0	305	0	0
	Γ_{8u}	2.727	0.004	307	831	596 [b]
$4f^1\ ^2F_{7/2}$	Γ_{7u}	2.724	0.001	307	2318	2125 [c]
	Γ_{8u}	2.727	0.004	307	3019	2686 [b]
	Γ_{6u}	2.727	0.004	307	3376	3083 [b]
$5d^1\ ^2T_{2g}$	Γ_{8g}	2.676	-0.047	293	25510	28195 [b]
	Γ_{7g}	2.676	-0.047	293	26716	29435 [b,d]
$5d^1\ ^2E_g$	Γ_{8g}	2.740	0.017	297	47263	47080 [c]

[a] Minimum-to-minimum energy differences.

[b] In Ce^{3+}/Cs_2NaYCl_6.

[c] In $Ce^{3+}/Cs_2NaErCl_6$.

[d] From Schwartz and Schatz[9]

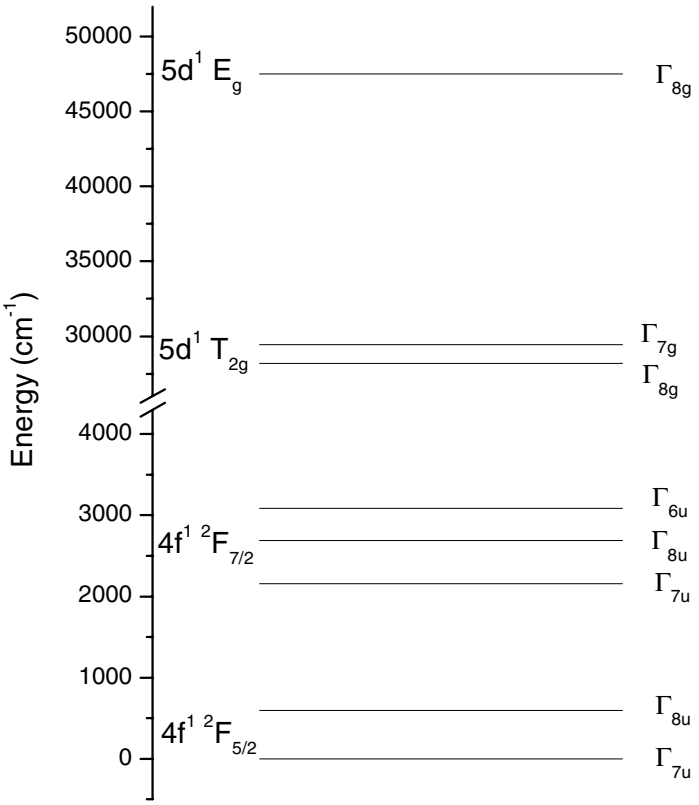

Figure 1 Schematic energy level diagram of the $4f^1$ and $5d^1$ configurations of the Ce^{3+} ion in a chloroelpasolite crystal field. Note the change in the energy scale between the $4f^1$ and the $5d^1$ configurations.

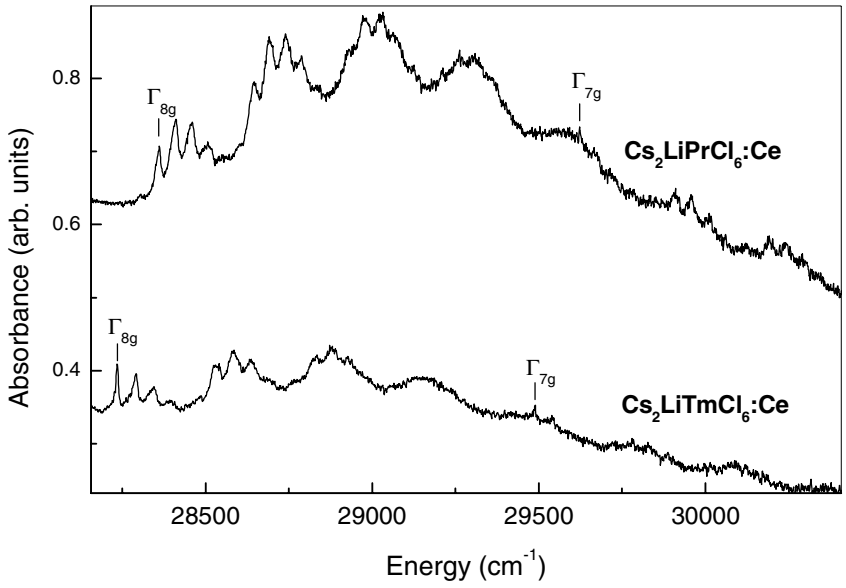

Fig. 2. 10 K absorption spectra of trace Ce^{3+} impurity in $Cs_2LiPrCl_6$ and $Cs_2LiTmCl_6$ between 28000 - 31000 cm^{-1}. (The initial state is Γ_{7u} in all cases, and the terminal d-electronic states are labeled).

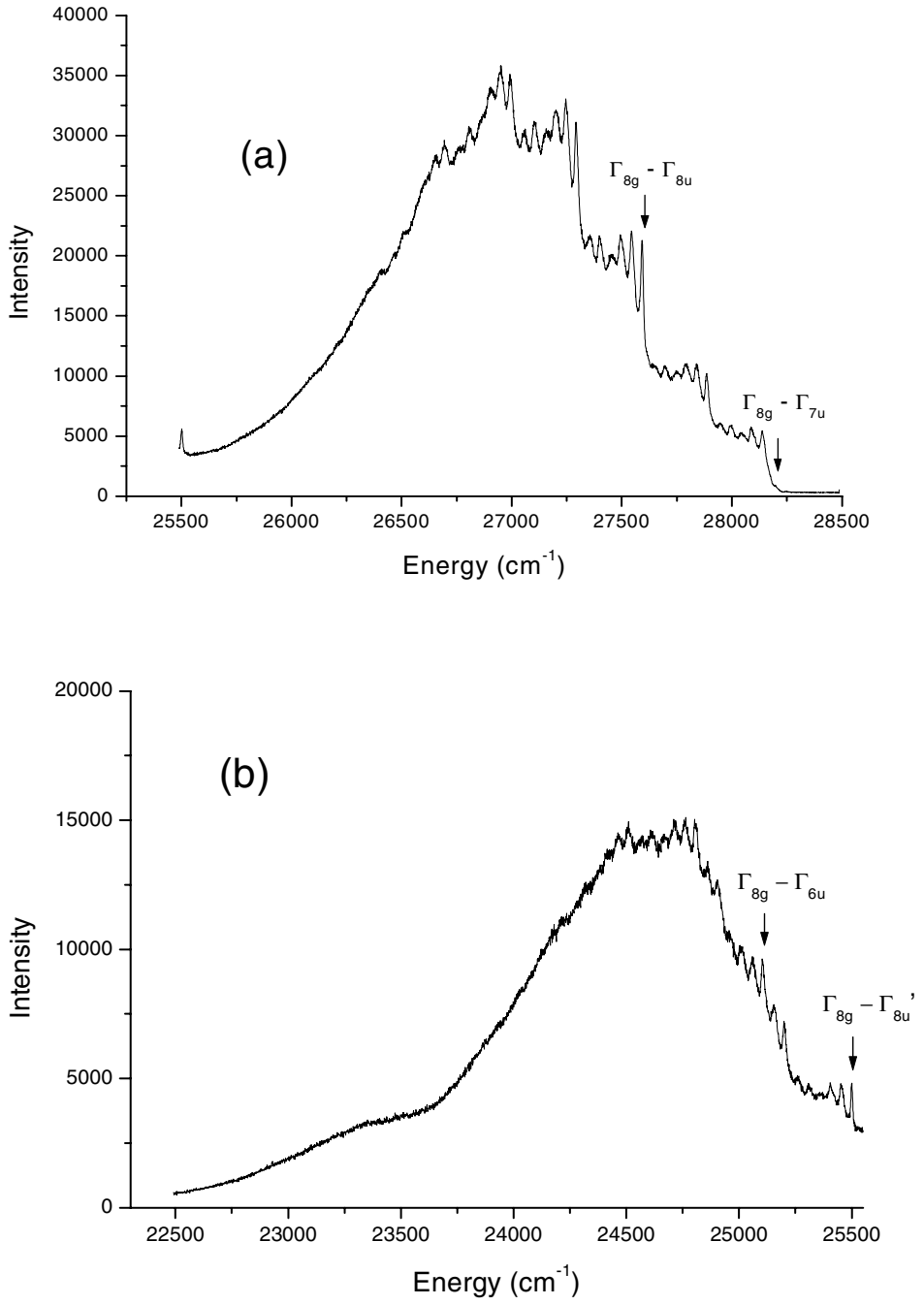

Fig. 3a,b. 10 K uv xenon lamp excited emission spectrum of Ce^{3+}/Cs_2NaYCl_6 between 28500 - 22500 cm^{-1}

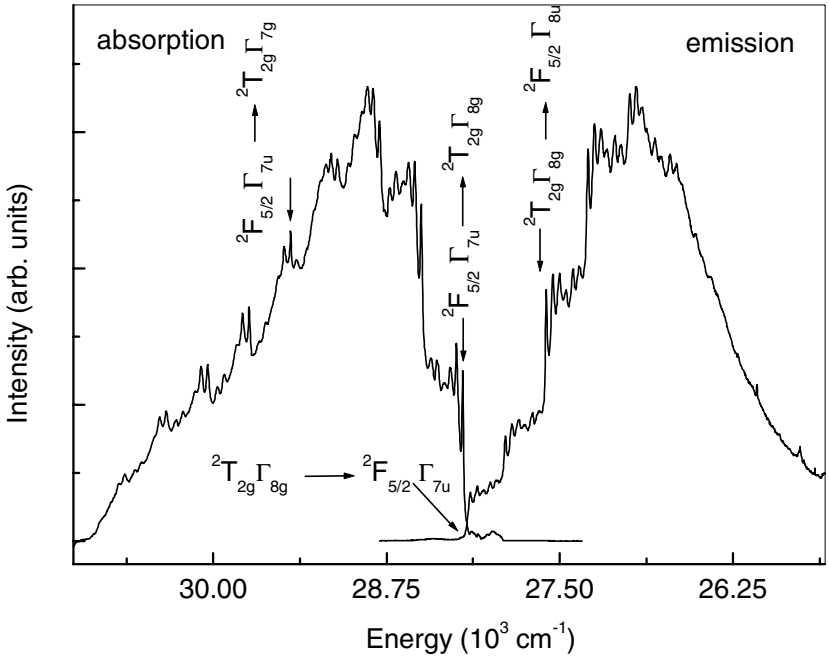

Fig. 4. Comparison of 10 K absorption spectrum of Ce^{3+}/Cs_2NaYCl_6 with the 199.8 nm excited emission spectrum at 10 K

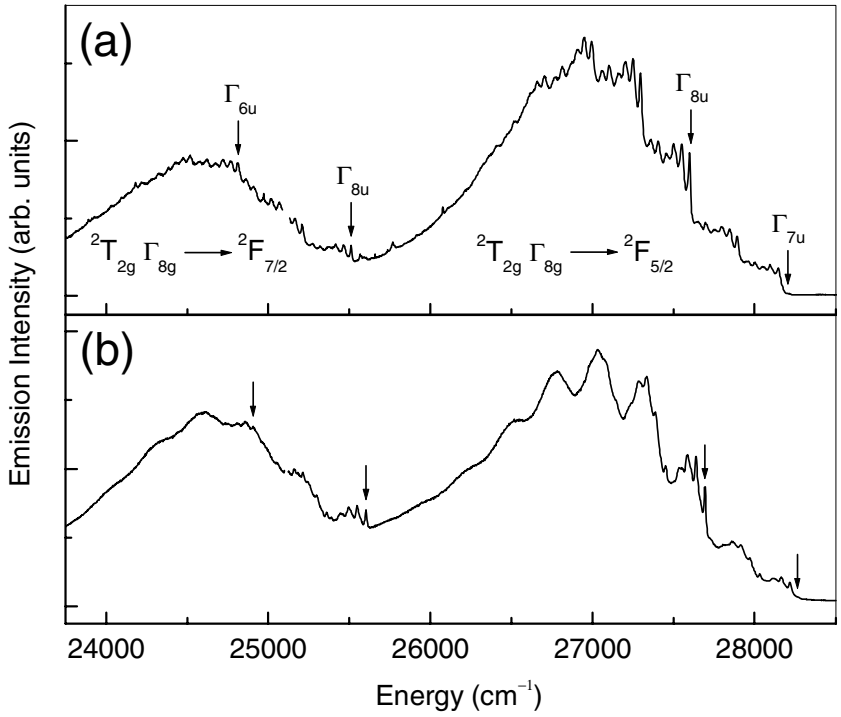

Fig. 5 Comparison of 199.8 nm excited 10 K emission spectra of (a) Ce^{3+}/Cs_2NaYCl_6 and (b) Ce^{3+}/Cs_2LiYCl_6. The terminal f-electron states are labeled.

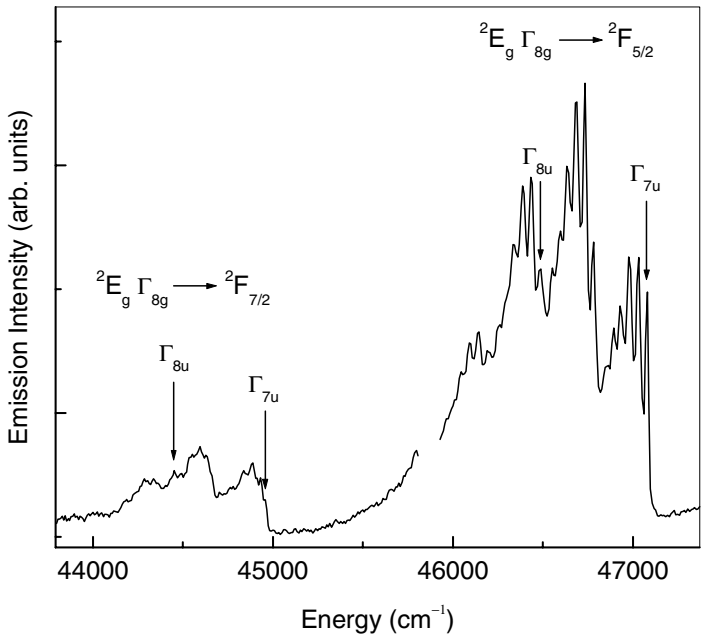

Fig. 6. 199.8-nm excited 10 K emission spectrum of $Ce^{3+}/Cs_2NaErCl_6$ between 47000 - 43500 cm^{-1}.

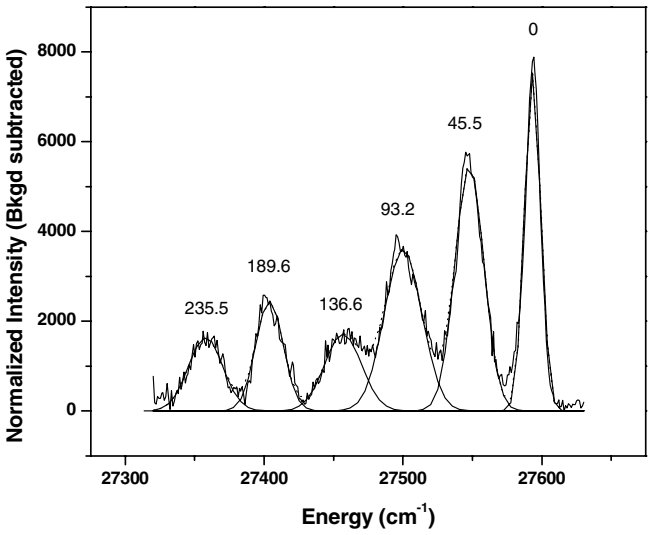

Fig. 7. Gaussian fits to the first few bands in the 10 K $^2T_{2g}\ \Gamma_{8g} \rightarrow {}^2F_{5/2}\ \Gamma_{8u}$ emission spectrum of Ce^{3+}/Cs_2NaYCl_6. The numbers over the centers of the bands indicate the energy intervals (in cm^{-1}) from the zero phonon line.

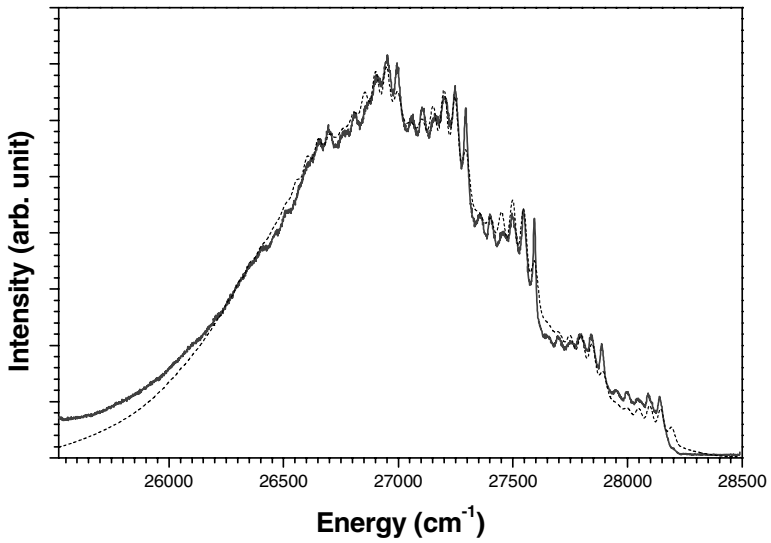

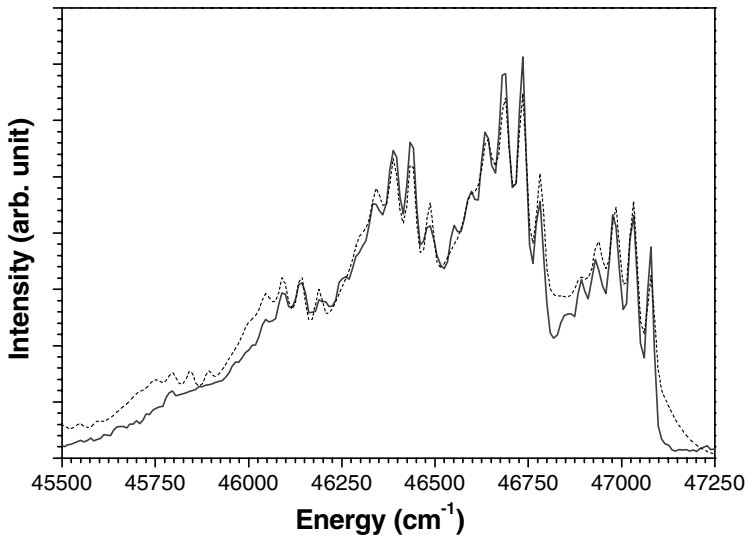

Fig. 8. Fits of the experimental emission spectra using the Huang –Rhys formulation as described in the text. Top) Ce^{3+}/Cs_2NaYCl_6: $S_{H\text{-}R1}$=1.275, ω_1=299 cm^{-1}, line width=14 cm^{-1}; $S_{H\text{-}R2}$=1.8, ω_1=47.5 cm^{-1}, line width=14 cm^{-1}; $S_{H\text{-}R3}$= 4.39, ω_1=202 cm^{-1}, line width=145 cm^{-1}; intensity ratio of the transitions $^2T_{2g}\,\Gamma_{8g} \rightarrow {}^2F_{5/2}\,\Gamma_{7u}$ to $^2T_{2g}\Gamma_{8g} \rightarrow {}^2F_{5/2}\,\Gamma_{8u}$ = 2.0. Bottom) $Ce^{3+}/Cs_2NaErCl_6$: $S_{H\text{-}R1}$=1.13, ω_1=297 cm^{-1}, line width=9 cm^{-1}; $S_{H\text{-}R2}$=1.3, ω_1=48 cm^{-1}, line width=9 cm^{-1}; $S_{H\text{-}R3}$= 1.55, ω_3=300 cm^{-1}, line width=105 cm^{-1}; intensity ratio of the transitions $E_g\,\Gamma_{8g} \rightarrow {}^2F_{5/2}\,\Gamma_{7u}$ to $E_g\Gamma_{8g} \rightarrow {}^2F_{5/2}\,\Gamma_{8u}$ = 0.13. The calculated spectra are shown as the dotted lines, the experimental data are shown as solid lines. Gaussian line shapes are assumed.

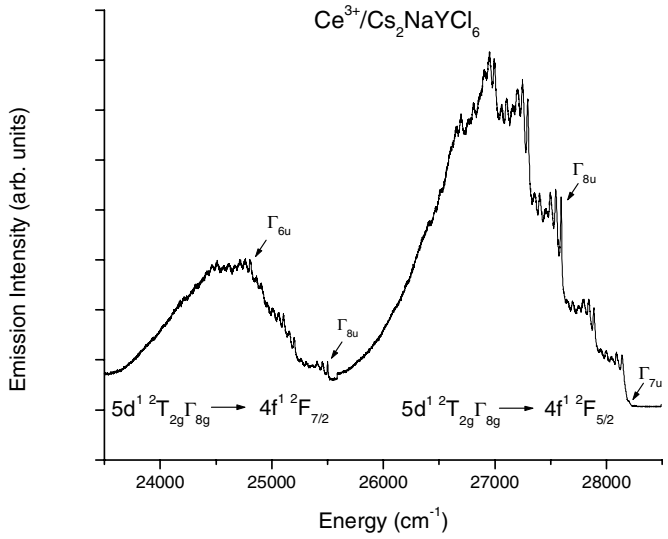
Ce3+/Cs2NaYCl6
Emission Intensity (arb. units)
Γ6u
Γ8u
Γ8u
Γ7u
5d1 2T2g Γ8g → 4f1 2F7/2
5d1 2T2g Γ8g → 4f1 2F5/2
24000
25000
26000
27000
28000
Energy (cm-1)

TOC Graphic